Neuron
Report

Vibrissal Kinematics in 3D: Tight Coupling of Azimuth, Elevation, and Torsion across Different Whisking Modes

Per Magne Knutsen,[1,4] Armin Biess,[2,3,4] and Ehud Ahissar[1,*]
[1]Department of Neurobiology
[2]Department of Mathematics
The Weizmann Institute of Science, 76100 Rehovot, Israel
[3]Max-Planck-Institute for Dynamics and Self-Organization, 37073 Göttingen, Germany
[4]These authors contributed equally to this work
*Correspondence: ehud.ahissar@weizmann.ac.il
DOI 10.1016/j.neuron.2008.05.013

SUMMARY

Perception is usually an active process by which action selects and affects sensory information. During rodent active touch, whisker kinematics influences how objects activate sensory receptors. In order to fully characterize whisker motion, we reconstructed whisker position in 3D and decomposed whisker motion to all its degrees of freedom. We found that, across behavioral modes, in both head-fixed and freely moving rats, whisker motion is characterized by translational movements and three rotary components: azimuth, elevation, and torsion. Whisker torsion, which has not previously been described, was large (up to 100°), and torsional angles were highly correlated with whisker azimuths. The coupling of azimuth and torsion was consistent across whisking epochs and rats and was similar along rows but systematically varied across rows such that rows A and E counterrotated. Torsional rotation of the whiskers enables contact information to be mapped onto the circumference of the whisker follicles in a predictable manner across protraction-retraction cycles.

INTRODUCTION

Most mammalian sensory systems process information collected through actively generated movements. The rodent vibrissal (whisker) system is a well-defined active sensing system where the musculature of the mystacial pad enables fine control of whisker movement for a variety of behavioral tasks (Brecht et al., 1997; Carvell and Simons, 1990; Herfst and Brecht, 2008; Knutsen et al., 2006). During passive stimulation, the primary sensory afferents of this system exhibit different tuning properties, such as selectivity for the direction of whisker deflection (Gibson and Welker, 1983; Lichtenstein et al., 1990), velocity thresholds (Arabzadeh et al., 2004; Jones et al., 2004), and preferred temporal frequencies of whisker deflections (Andermann et al., 2004). Recently, studies in actively sensing rats have demonstrated that neuronal activity is significantly influenced by motor activation (Ferezou et al., 2007; Krupa et al., 2004; Szwed et al., 2003; Yu et al., 2006). Patterns of head and whisker movements have been shown to vary across different behavioral tasks. During horizontal object localization, rats reduce head movements and increase whisker movements (Knutsen et al., 2006), while, during radial object localization, whisker movements are suppressed and head movements become more important for accurate sensing (Krupa et al., 2001).

In order to examine how whisker motion may constrain sensory activation, we analyzed different kinematic features of whisking while head-fixed or freely moving rats were whisking in free air or during an object localization task, respectively. Previously, it has been shown that natural whisker movements are not confined to a single plane but that the whiskers move in at least two dimensions: horizontal and vertical (Bermejo et al., 2002). Here, through full 3D reconstructions of whisker movement, we described all rotational components of whisker movement, including a hitherto unknown torsional rotation of the whisker shaft. Whisker torsion is a rotary motion of the whisker shaft around its own axis, and was observed during different modes of active sensing in the awake, behaving rat. We found that the components of whisker motion are highly coordinated, thus reducing the free variables involved in whisker movement control. We propose a scheme by which this simplified scheme of motor control enables directional selectivity of sensory neurons to be used in object localization and texture coding.

RESULTS

Reconstructions of Whisker Shapes in 3D

We measured all components of rat whisker movement using 3D high-speed video (Figure 1A). Awake rats were head restrained, and a single whisker was marked with dye at three to five locations along the shaft (between 10%–70% of the whisker length). The thinness of the distal part of the whisker shaft precluded us from applying markers beyond ~70% of the whisker length. Thus, we focus here on the proximal 70% of the whisker shaft. Spontaneous whisker movements were monitored from two different camera angles, permitting 3D reconstructions of the whisker shaft by matching corresponding markers across the

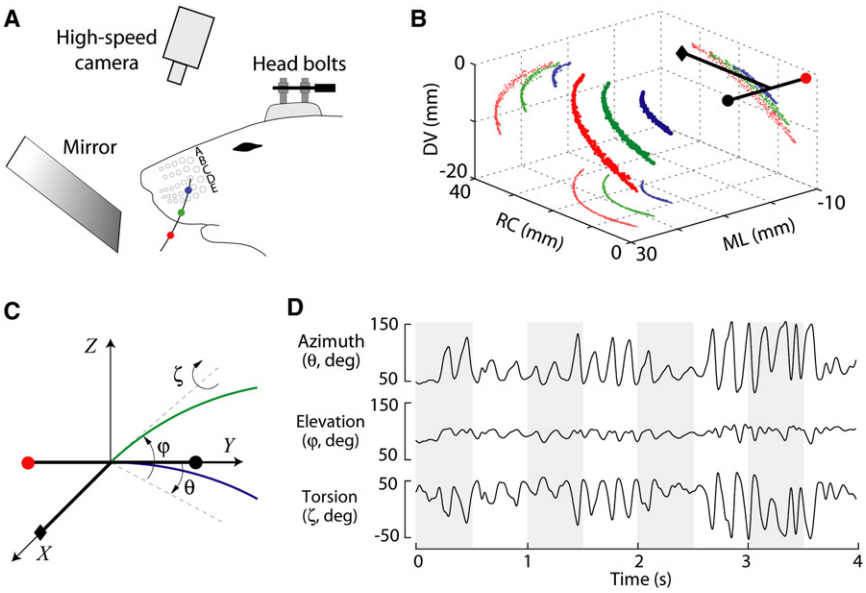

Figure 1. Measurements of 3D Whisker Movements

(A) Head-fixed rats were positioned under a high-speed camera and in front of a mirror. Whisker rows are named A to E, from top to bottom. Whiskers were labeled at three to five locations along the shaft with small drops of ink (colored dots), and 3D locations of labels were computed from matched 2D coordinates.

(B) 3D reconstruction of a C1 whisker in head-centered coordinates. Axes denote dorsoventral (DV), rostrocaudal (RC), and mediolateral (ML) locations of the labels relative to the head (black circle, left eye; red circle, right eye; diamond, nose). Whisker labels in 3D are represented by thick colored dots, and projections to the horizontal, coronal, and sagittal planes by thin dots. Data shown include 1.7 s of whisking (ten cycles; see Movie S1).

(C) Coordinate system used for measurements of angular whisker rotations. A whisker reconstructed in 3D was first translated to the origin, located half-way between the eyes, in a head-centered coordinate system (x, y, z). The angular orientation of the whisker (green) was then determined with respect to a trial-specific reference whisker (blue, see Experimental Procedures) in the y z plane that had a tangent vector at the base in the direction of the y axis. The whisker orientation in each frame was specified by azimuthal (θ), elevation (φ), and torsional (ζ) angles. Dots and diamond indicate positions of the eyes and nose (as in [B]).

(D) Rotational movements of an A1 whisker throughout an episode of continuous whisking. All angular movements are shown to scale.

two images obtained in each video frame (Figure 1B and see Movie S1 available online). In each movie, the intrinsic 3D shape of the whisker shaft was estimated by fitting a quadratic curve, $\boldsymbol{X}(u) = \boldsymbol{a} + \boldsymbol{b}u + \boldsymbol{c}u^2$, to the reconstructed 3D locations of the most proximal, the most distal, and one of the middle markers in the first video frame ($f = 1$). The exact same quadratic function, with the same parameter values, was then used in all subsequent movie frames ($f = 2, \ldots, K$) by finding the best fit in a least-squares sense to the marker locations in 3D. We assumed, therefore, that the intrinsic shape of a whisker did not change in the course of a whisking epoch. We confirmed this assumption by measuring the error of the fit to the whisker markers, in 3D, in frames $f = 2, \ldots, K$. Fitting the exact same quadratic curve across all frames resulted in average residuals of 0.09 ± 0.08 mm (mean ± SD). We compared these residuals to the accuracy of our 3D reconstruction method, which was measured by the Euclidian distances between points on a calibration target of known dimensions (see Experimental Procedures for details). Overall, the discrepancy between real and computed 3D points on the calibration target was 0.16 ± 0.13 mm. In all reconstructed trials, the residuals of the quadratic whisker shaft fits were never significantly larger than this calibration error ($p < 0.05$; Wilcoxon). Thus, we conclude that (1) the shape of the whisker shaft (0%–70% of whisker length) can be idealized as a quadratic curve, thus (2) by definition, the whisker must be said to lie flat in a plane, and (3) the intrinsic shape of the whisker shaft (within the limits of our method) does not change during free-air whisking.

Whisker Rotations during Free-Air Whisking

We recorded a total of 141 spontaneous whisking bouts performed by head-fixed rats, totaling 900 s of whisking behavior. Movements of whiskers in all rows and arcs 1–3 were reconstructed in 3D. These reconstructions permitted us to decompose five parameters that describe a whisker's position and orientation in 3D space, including translations of the whisker base (horizontal and vertical) and rotations of the whisker shaft (azimuth, θ; elevation, φ; and torsion, ζ). Here, we describe the time-varying fluctuations of whisker azimuth, elevation, and torsion during free-air whisking, as shown for whisker A1 in Figure 1D (see also Movie S1). The commonly described back-and-forth movement is captured by the whisker azimuth, which in Figure 1D varies significantly in amplitude though not in frequency. Whisking epochs ranged from 0.5–20 s, and whisking frequencies were narrowly distributed in a 5–10 Hz band (7.5 ± 2.9 Hz), as previously reported for head-fixed rats whisking in free air (Gao et al., 2001).

Consistent with a previous report (Bermejo et al., 2002), we found that a change in whisker azimuth was correlated with a change of whisker elevation during whisking [R^2 = 0.96 ± 0.27 across all whiskers; see also column $R^2(\theta, \varphi)$ in Table 1]. During the protraction phase of whisker movement, the elevation of all whiskers, except whiskers in the E row, increased. Whiskers in row E went through negligible changes in elevation angles during protraction (see Table 1). The proportion of change in elevation during protraction (the slope $\Delta\varphi/\Delta\theta$) was maximal in rows B and C (~30%) and progressively smaller in the upper and lower whisker rows (A, D, and E; Table 1).

The absolute elevation varied consistently across whisker rows. According to our conventions, zero elevation denotes the plane defined by the two eyes and nose. Thus, when a whisker is pointed upward relative to this plane, elevation is positive. Conversely, when a whisker points downward, elevation is negative. When the whiskers were in their primary, retracted position, whisker elevation changed gradually from positive in the

Table 1. Whisker Elevation during Rest and Active Whisking (Degrees)

Row	Rest elevation[a]	$\Delta\varphi/\Delta\theta$[b]	$R^2(\theta,\varphi)$[c]
A	56 ± 5.3	0.12 ± 0.17	0.82
B	25 ± 9.4	0.30 ± 0.17	0.96
C	−4.2 ± 6.3	0.30 ± 0.13	0.99
D	−27.2 ± 7.7	0.14 ± 0.14	0.90
E	−44 ± 7.6	−0.02 ± 0.13	0.71

[a] The rest position was defined as the average (mean ± SD) elevation of the whiskers at the onset of all whisk cycles. Angles were averaged across whiskers of the same row. Zero elevation corresponds to an angle parallel to a plane intersecting both eyes and nose of the rat.
[b] The average rate of whisker elevation during protraction, expressed as the change of elevation divided by the change of whisker azimuth (mean ± SD).
[c] Average correlation coefficients (R^2) between whisker azimuth and elevation.

upper-most A row (56° ± 5.3°) to negative in the lower-most E row (−44° ± 7.6°). We found no significant variations in whisker elevation within individual whisker rows.

Torsional Rotation of the Whisker Shaft

Whisker torsion is a rotary motion of the whisker shaft around its own axis (Figure 1C, ζ; see Movie S2 for a graphic visualization of torsional rotation). We observed torsional rotation of all measured whiskers (rows A–E and arcs 1–3) in all whisking epochs (n = 7 rats). Figure 2A illustrates the relative phase and amplitude of whisker azimuth and torsion for all arc 1 whiskers in five different whisking epochs. Overall, the linear correlation between whisker azimuth and torsion was high ($R^2 \geq 0.74$ in Figure 2B). Thus, we quantified torsional rotation during free-air whisking by the slope (m) of a straight line fitted between azimuth and torsion of individual whisk cycles (n = 574, where all whisks had amplitudes ≥30° azimuth); m would have values close to 1 for correlated rotations and close to −1 for anticorrelated rotations. Within rows, m was similar across individual whiskers ($p > 0.05$, Wilcoxon), with the exception of row C where m of whisker C2 ($m = 0.29 \pm 0.23$) was greater than for other whiskers in the same row ($m = 0.14 \pm 0.17$; $p < 0.001$). The direction and amplitude of torsion varied significantly across whisker rows. Figure 2C summarizes the average torsional angle (represented by the orientation of arrows) of same-row whiskers as a function of whisker azimuth. According to our conventions, when the rat is seen from the side and its nose faces right, a reduction in torsional angle implies clockwise rotation of the whisker shaft, while an increase in torsional angle implies anticlockwise rotation. This representation demonstrates that when the whiskers move from maximal retraction (~45° azimuth) to maximal protraction (~150° azimuth) the upper (A and B) and lower (C, D, and E) rows counterrotate; upper rows decrease and lower rows increase their torsional angles. The planes that represent the torsional orientation were aligned only about half way (~110° azimuth) across the azimuthal range.

During protraction, torsional whisker angles always decreased in row A ($m = -0.76 \pm 0.08$), usually decreased in row B ($m = -0.25 \pm 0.18$), usually increased in row C ($m = 0.22 \pm 0.22$), and always increased in rows D and E ($m = 0.42 \pm 0.11$ and 0.73 ± 0.14, respectively; Figure 2D). The torsion-azimuth ratio (m) was significantly different between all neighboring whisker rows ($p < 0.001$, Wilcoxon) and had the highest absolute values in the most upper (A) and lower (E) whisker rows. Overall, the torsional angle could be described as varying linearly with the azimuth angle of the whiskers during whisker protraction (Figures 2B and 2E). In whisker rows B and C, however, the relationship between torsion and azimuth was better described by a quadratic fit (red lines in Figures 2B and 2E). Averaging across all rows revealed that each whisker on average scanned through 34° ± 17.5° of azimuth, 13° ± 7.9° of elevation, and 31° ± 22.4° of torsional rotation in individual whisk cycles (mean ± SD). Whisker rotation set-points and amplitudes varied between different whisk cycles of each bout (see example in Figure 1D). The total range scanned by whiskers in individual whisking bouts, given by the difference between maximal and minimal angles during a bout, was significantly larger than that scanned during individual cycles ($p < 0.001$). On average, an individual whisker scanned through 76.2° ± 24.6° of azimuthal rotation, 31° ± 13.9° of elevation, and 60.5° ± 48.4° of torsional rotation (mean ± SD; Figure 2F) during a single bout.

Estimating Whisker Torsion from a Single Vantage Point

Previously (Knutsen et al., 2005), we have described that the projected whisker curvature (κ_{top}), when viewed from top to down, varies systematically during protraction and correlates with the projected whisker angle (θ_{top}, Figure 3A). Such variations could result from bending of the whisker shaft, translations of the shaft relative to the viewing angle, or torsional rotation of the whisker shaft. As described above ("Reconstructions of Whisker Shapes in 3D), we found that bending of the whisker shaft is negligible during free-air whisking. Recently, we have reported that, while rats perform a bilateral object localization task, head translations do not correlate significantly with whisker movement on a cycle-to-cycle basis (Knutsen et al., 2006). Thus, neither whisker bending nor translation of the whisker shaft due to head movements could account for the variations in projected curvature. Instead, we examined whether torsional whisker rotation could be inferred from high-speed movies capturing a top-down view of the whiskers in head-restrained rats. Whisker torsion (ζ) was measured by decomposition of the rotational movements of 3D reconstructed whiskers, and the projected whisker curvature (κ_{top}) was obtained from the top-down view used for the 3D reconstruction. Figure 3B shows the torsional angle and the top-down projected curvature of a C1 whisker across 500 ms of whisking. In this example, whisker torsion and the projected curvature were highly correlated ($R^2 = 0.90$, $p < 0.001$, Figure 3C). Across all recorded whisking bouts, correlations between torsional rotation and top-down projected curvature were high (median $R^2 = 0.80$, $p < 0.01$, n = 818 whisks; Figure 3D). Thus, the top-projected curvature, κ_{top}, is a reliable indicator of torsional rotation.

Whisker Torsion during Object Localization by Freely Moving Rats

In order to examine whether torsional rotation of the whisker shaft is a ubiquitous phenomenon and not limited to head-fixed

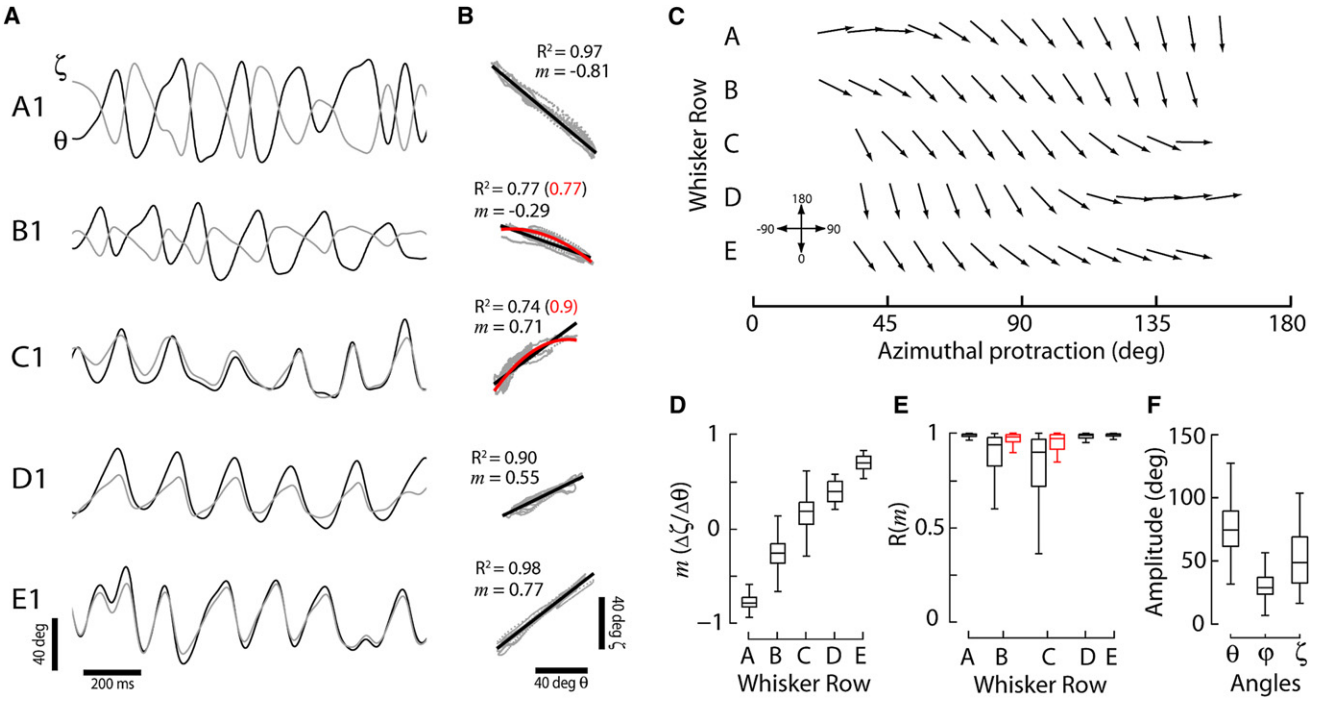

Figure 2. Correlations between Whisker Azimuth and Torsion

(A) Azimuth (θ; black) and torsion (ζ; gray) of all arc 1 whiskers during whisking. Each trace was obtained from a different whisking episode.

(B) Linear (black) and quadratic (red) least-squares fits to θ and ζ data in (A).

(C) Average torsional angle at different whisker azimuths across all whisker rows. Whisker azimuth and torsion were averaged in bins of 10° azimuth and then across all whiskers in the same row. An arrow indicates the torsional orientation of the plane containing the whisker shaft at the indicated azimuth angle.

(D) Box plots of the ratio of torsion to azimuth rotation (m) during individual whisk cycles. Boxes indicate the interquartile range, middle lines the medians, and vertical lines the range of data.

(E) Box plots of correlation coefficients (R) of linear (black) and quadratic (red) least-squares fits to θ and ζ during whisker protractions (see examples in [B]). Correlation coefficients in rows A, E, and D were high (R = 0.95 ± 0.13; mean ± SD) but substantially lower for rows B and C (R = 0.72 ± 0.3). Thus, distributions of R obtained from quadratic fits are shown only for rows B and C (R = 0.88 ± 0.18).

(F) Range of whisker angles (θ, φ, and ζ) spanned during whisking epochs (n = 94 whisking bouts).

animals whisking in free-air, we inferred torsional rotation from the top-down projected whisker curvature (κ_{top}) of freely moving rats performing an object localization task (Knutsen et al., 2006). Figure 3E illustrates the time-varying top-down projected whisker curvature (κ_{top}) and angle (θ_{top}) of the right and left C1 whiskers while a rat was discriminating the relative horizontal distances of two vertical poles. During protraction in free air, the C1 whisker always reversed from a concave to a convex shape in the anterior direction (Figure 3F, top and middle panels). Upon contact, the whisker bent and became more concave (Figure 3F, bottom). However, prior to object contact and immediately after detach, torsional angles were typically close to each other, suggesting that the torsional angle prior to contact was maintained also during object-induced bending of the whisker shaft (Figure 3E). The changes in projected curvature correlated with whisker angle on a cycle-by-cycle basis (Figure 3G), implying torsional rotation of the whiskers in a manner comparable with that observed in head-fixed rats (Figures 2A, 3B, and 3C).

All 3D reconstructed whiskers in the head-fixed rat were intrinsically curved with the tip toward the ground (i.e., convex relative to ground; Figure 3H). Thus, the direction of torsional whisker rotation in the freely moving rat can be unambiguously deduced from the change in the projected curvature, $\Delta\kappa_{top}$, as only an increase in torsional angle could lead to an increase in convexity ($\Delta\kappa_{top}<0$) of a whisker viewed from top. From this, it follows that the torsional angle of both C1 whiskers in Figure 3E increased during protraction and decreased during retraction, as was also observed in the head-fixed whisking rat (Figures 2A–2C). We measured the direction of the curvature change, and thus also torsional rotation, during protractions ($\Delta\theta_{top}>0$) of whiskers B1, C1, and D1 (Figure 3I). In the case of B1, the top-down projected whisker shape became more concave upon protraction ($\Delta\kappa_{top}>0$), implying that the torsional rotation of this whisker was negative. In the case of both C1 and D1, the whisker shape became more convex during protraction ($\Delta\kappa_{top}<0$), implying that the torsional angle of these whiskers increased during protraction.

DISCUSSION

Control of Whisker Torsion

We found that the whiskers undergo torsional rotation during natural whisking behavior and that such rotation was not restricted to any specific behavioral mode. Torsional rotations

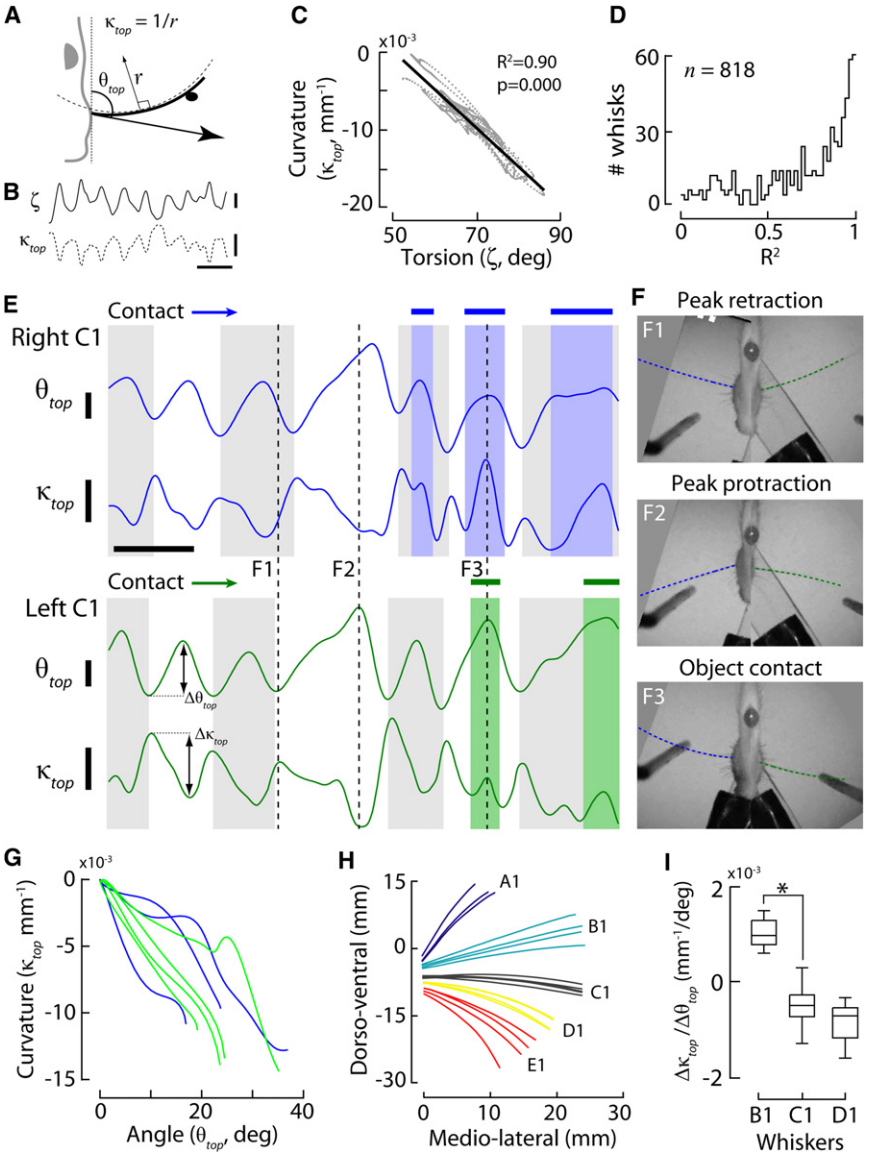

Figure 3. Torsional Whisker Rotation during Object Localization

(A) Measurements of whisker azimuth (θ_{top}) and curvature (κ_{top}) from the top-down projection of a whisker fitted by piecewise polynomials (Knutsen et al., 2005). Whisker azimuth was approximated as the tangent angle of the whisker base, and whisker curvature as the inverse of the maximal radius along the whisker shaft (r). Black thick line illustrates the whisker, black dot an object, large arrow the azimuth, and the dotted semicircle the whisker radius (not to scale).

(B and C) Torsional angle (ζ, top) and top-down projected curvature (κ_{top}, bottom) of a C1 whisker belonging to a head-fixed rat. Whisker torsional rotation was obtained through 3D reconstruction and curvature from a top-down view of the whisker. Calibration bars indicate 10°, 0.01 mm^{-1} curvature, and 100 ms.

(D) Distribution of correlation coefficients (R^2) obtained from linear regressions between whisker torsion and projected curvature during whisker protractions (as in [C]).

(E) Top-down projected whisker azimuth (θ_{top}) and curvature (κ_{top}) of a freely moving rat during an object-localization trial. Right (blue) and left (green) C1 whiskers were tracked in a head-centered reference frame. Alternating gray/white back-shading indicate consecutive whisk cycles. Colored back-shading and thick bars above the traces indicate intervals when a whisker contacted a vertical pole. Dashed, gray vertical lines (numbered F1–F3) indicate moments of the frames in (F). Calibration bars indicate 10° azimuth, 0.01 mm^{-1} curvature, and 100 ms.

(F) Frames showing different events during the same object localization trial as in (E). Images were cropped relative to head location and then aligned such that both the ipsilateral eye and nose fell on the ordinate. (Top) Whisker positions at peak retraction. Whisker projections were concave, indicated by negative curvature values in (E). (Middle) Whiskers at peak protraction. Projected whisker shapes were convex. (Bottom) Bending of whiskers upon contact, resulting in concave whisker shapes.

(G) Projected whisker curvature versus azimuth in all noncontacting protraction cycles in (E) (one line for each cycle). For comparison, all cycles were shifted to the origin.

(H) Front-to-back projections of arc 1 whiskers, obtained by reconstructing whisker shafts of head-fixed rats in 3D. Front-to-back projected shapes were averaged across frames when the whisker azimuth was 90°. Each line is the front-to-back projection of an individual whisker.

(I) Box plots of relative change in top-down projected curvature during whisker protraction ($\Delta\kappa_{top}/\Delta\theta_{top}$) for B1 (n = 103 whisks from four whiskers), C1 (n = 1281 whisks from 12 whiskers), and D1 (n = 61 whisks from four whiskers). $\Delta\theta_{top}$ and $\Delta\kappa_{top}$ are the differences in top-down projected angle and curvature (see [A]), respectively, between peak-retraction and peak-protraction. Boxes indicate the interquartile range, middle lines the medians, and vertical lines the range of data.

were observed during movements of all monitored whiskers, in all whisking epochs, and in all tested rats. Also, we observed (directly or inferred) torsion both in head-fixed whisking in free air and freely moving rats performing an object localization task. Previously, we have also described changes in the projected whisker curvature, consistent with torsional rotation, in freely moving rats whisking in free air (Knutsen et al., 2005). Thus, whisker torsion appears to be ubiquitous and not the outcome of restraint or specific perceptual requirements.

The high correlation between whisker azimuth and torsion (Figure 2E) and projected whisker angle and curvature (Figure 3G) argues against independent control of torsion in the motor output. In the oculomotor system, the rotation of the eye around its visual axis (torsion) is determined by the azimuth and elevation of the eye (expressed by Donder's and Listing's laws). In the vibrissal system, however, we find that whisker torsion, as well as elevation, is fully determined by the azimuth angle alone during whisker protraction. Thus, the whisker version of Donder's law can be expressed as $\zeta = \alpha\theta + \beta$ for whiskers in rows A, D, and E and $\zeta = \gamma\theta^2 + \alpha\theta + \beta$ for whiskers in rows B and C (Figure 2). This simple relationship suggests that torsional rotation is mechanistically implemented by neuronal correlations or by neuromuscular constraints imposed by the structure of the mystacial tissue and musculature. Some evidence suggests that

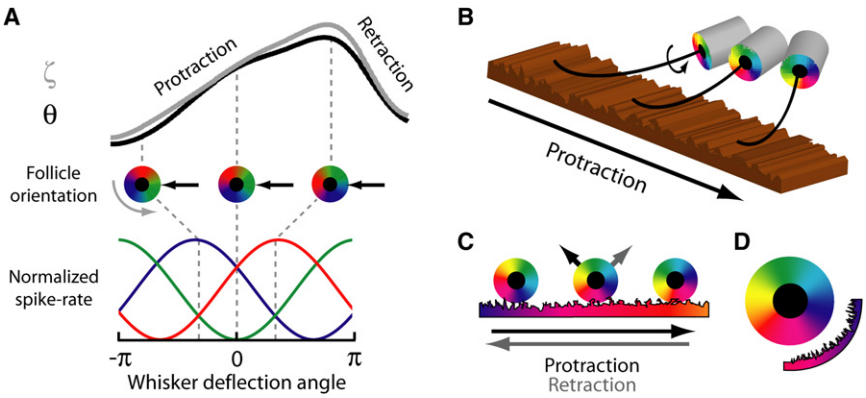

Figure 4. Mapping of Angular Phase to Neural Activity

(A) (Top) Real case of correlated whisker azimuth (θ; black) and torsion (ζ; gray) during protraction. (Middle) Cross-section of whisker follicle. Change in whisker torsion rotates the follicle around its own axis (gray arrow). When the whisker (black dot) contacts an object, a reaction force acts upon the shaft (black arrows). The direction of the reaction force in whisker coordinates is determined by the torsional angle and follicle orientation. (Bottom) Hypothetical directional tuning curves of three sensory afferents. Firing rate of these units at different moments of contact (gray dashed lines) with an object is determined by the reaction force vector in whisker coordinates, determined by ζ during whisking.

(B) 3D schematic of follicle and whisker orientation during scanning of a textured surface.

(C) Orientation of a follicle (color wheels) relative to a surface at three different times during protraction and retraction. During protraction (black arrows), reaction forces activate directionally tuned afferents on one side of the follicle. During retraction (gray arrows), reaction forces change direction and thus activate different afferents. Due to torsional rotation during both phases of motion, the identities of activated afferents will smoothly change across a range determined by the torsional amplitude.

(D) As a result of whisker torsion, surface details are mapped onto the circumference of the follicle.

torsional rotation of the whiskers may rely, at least in part, on asymmetric motor innervation received by the vibrissal musculature (Dorfl, 1985).

Functions of Whisker Torsion

The limited space allows a discussion of only a few possible functional consequences of torsional whisker rotation. The arrangement of torsional rotations implies that reaction forces are maximized when upward-facing surfaces (e.g., ground) are scanned by whiskers in rows C–E and downward-facing surfaces (e.g., ceiling) are scanned by rows A and B.

When a whisker rotates around its own axis during protraction, its orientation relative to a fixed object continuously changes. The torsional angle of the whisker upon contact with the object determines the direction of the reaction force applied to the whisker shaft. The whisker follicle is innervated by primary afferent nerves, whose directional tunings have been shown to match the location of their follicular innervation zones (Waite and Jacquin, 1992). Thus, when a whisker is mechanically deflected in different directions, resulting in different circumferential pressure profiles on the follicle, the degree of activation of each primary afferent is altered (Gibson and Welker, 1983; Lichtenstein et al., 1990).

During active touch, the torsional angle upon contact with an object determines the circumferential pressure profile and therefore also the spatial activation profile of the primary afferent population. Thus, contact at different torsional angles is associated with different activity profiles across all directionally tuned primary afferents (Figure 4A). Since torsion is coupled with azimuth, this spatial encoding of the torsional angle also transmits information about the degree of whisker protraction and could thus be used to encode the horizontal location of objects. Also, whisker torsion could account for the reported encoding of protraction angle by whisking-selective cells (Szwed et al., 2003), since rotation of the follicle may cause different muscle-induced strains on mechanoreceptors located around the follicle circumference.

Due to the ubiquity of torsional rotation across different behavioral conditions, it is likely that the strong correlation between azimuth and torsion is also present under conditions we did not test. One whisking mode of particular relevance is the scanning of textured surfaces (Arabzadeh et al., 2005; Carvell and Simons, 1990, 1995; Ritt et al., 2008; von Heimendahl et al., 2007). When a whisker is moved along a surface, the direction of the normal surface reaction force relative to the follicle rotates continuously, along with torsional rotation (Figures 4B and 4C). As a result, the mechanical details of the surface are mapped onto the circumference of the follicle (Figure 4D). Potentially, this peripheral mapping can induce mapping of texture details onto cells with different directional selectivities along the long axis of individual barreloids in the thalamus in every whisking cycle (Timofeeva et al., 2003).

The activation of primary afferents can be characterized in three domains: (1) the intensity of activation, measured in spikes/s, (2) the timing of firing, and (3) the spatial profile of activated afferents. These domains are affected by both motor activation and object properties. Vibrissal motor activation is characterized by five movement components: three rotational (azimuth, elevation, and torsion) and two translational components (horizontal and vertical). Azimuthal rotation of the whisker and its temporal derivatives are probably the primary motor variables affecting the timing and intensity of afferent activation (Szwed et al., 2003, 2006). Here, we found that torsional rotation of the whisker shaft, which affects the spatial activation pattern of primary afferents in each follicle, is highly correlated with whisker azimuth during protraction. Thus, the motor contribution to activation of primary afferents in all primary domains (timing, intensity, and identity) is in effect determined by temporal derivatives of a single controlled parameter in the motor output, namely whisker azimuth. We propose that this reduction of motor variables simplifies sensation-targeted motor control and thus facilitates perceptual stability and sensory integration across sequential protraction/retraction cycles. Future studies should be aimed at testing these

hypotheses directly, by measuring the activation of primary afferents during object contact across a wide range of whisker angles.

EXPERIMENTAL PROCEDURES

Surgery

During anesthesia (pentobarbitone 35 mg/kg, I.P.), 7 female Wistar rats (200–300 g) were fitted with a dental acrylic cement stage (Jet Acrylic; Lang Dental Mfg. Co., Inc.; Wheeling, IL), attached to the skull with miniature screws (MX-0080-02B; Small Parts Inc.; Miami Lakes, FL) and 4-META containing resin (Chemiace II; Sun Medical Co., Ltd; Moriyama, Japan). Two mounting screws were embedded in the cement for head immobilization. Rats were postoperatively treated with antibiotics (penicillin and streptomycin; Pen-Strep, 2 ml/kg S.C.) and analgesics (carprofen; 5 mg/kg S.C.). Rats were housed individually and maintained within 85% of free-feeding weight.

Monitoring of Whisker Movements

For measurements of whisker movements during head restraint, rats were gradually acclimatized to immobilization, first by handling (30 min/day, 3 days), and then restrained inside a 20 × 6 mm plastic tube. Rats were head fixed using an articulated manipulator (NF60103; Noga Engineering Ltd.; Schlomi, Israel). Fruit juice was presented throughout experiments to reduce stress. All but one to three whiskers on the right mystacial pad were trimmed down to the skin, and small drops of a metallic marker dye (Artline 990XF; Shachihata; Nagoya City, Japan) were applied at three to five locations along the shaft of a single whisker. Application of the dye increased whisker weights by <5% and did not result in any detectable change in the intrinsic whisker shape. Movements of 12 different whiskers were tracked: A1-2, B1-2, C1-3, D1-3, and E1-2. Whiskers posterior to arcs 2–3 were not tracked, as labeling these significantly increased their weight. The whisker field was backlit using a custom-made array of LEDs (L940-04AU, Epitex; Kyoto, Japan) or a cold light (Alpha-1501; LW Scientific, Ltd.; Lawrenceville, GA), and a high-speed video camera (MotionPro, Redlake; San Diego, CA) captured spontaneously occurring whisking bouts at 1000 frames/s (6.3 ± 2.3 s duration). Movements of the whisker-attached dye marks were automatically tracked offline using custom-written MATLAB software (Knutsen et al., 2005). On average, seven movies were acquired in each session (30–45 min), and 141 videos were acquired across all 22 experiments (~15 min of whisking activity).

We also analyzed head and whisker movements of freely moving rats performing a horizontal object localization task. Details on the localization task have previously been described in Knutsen et al. (2006). In brief, 34 Wistar rats were trained in a two-alternative forced-choice task to discriminate the relative horizontal offset of two vertical poles. The rats were conditioned to approach a discrimination area and nose-poke a contact switch while palpating the objects with their whiskers. Rats were rewarded with fruit juice for correctly discriminating the relative anterior-posterior locations of the poles. Head and whisker movements executed during object localization were recorded at 500 frames/s with a high-speed camera placed above the rat, looking down. Frame-by-frame whisker position was estimated by fitting piecewise polynomials to imaged whisker shafts using custom routines implemented in MATLAB (Knutsen et al., 2005). Whisker tracking from a top-down view allowed us to estimate the whisker azimuth and the shape of the whisker shaft (Figure 3A). Whisker azimuth was approximated by measuring the tangent angle at the base of the projected whisker (θ_{top}). For camera orientations with image planes parallel to the x y axes of the head-centered coordinate system, this angle reflects the true azimuth θ up to an unknown angular shift (c). Thus, we report only the approximate whisker azimuth (θ_{top}) in these experiments. Whisker torsion was inferred from the top-down projected curvature (κ_{top}) of the whisker shaft ($\kappa_{top} = 1/r$, where r is the maximal radius encountered along the whisker shaft).

3D Reconstructions

Whisker movements were reconstructed in 3D using a stereo-matching method. In brief, the whiskers were imaged simultaneously from top-down and front-to-back with the aid of a mirror (NT40-042; Edmund Industrial Optics; Barrington, NJ). Movements of the whisker-attached dye marks were tracked offline, the corresponding dye marks matched across the two camera views, and 3D locations of the dye marks then estimated based on epipolar geometry (Hartley and Zisserman, 2000). The intrinsic shape of the whisker shaft was estimated by fitting a quadratic parametric curve through the reconstructed dye marks in 3D. Calibration points permitted 3D coordinates of the whisker shaft to be expressed in head-centered coordinates. Rigid motion of whisker shaft was decomposed into translation (horizontal and vertical) of the whisker base and rotation (azimuth, elevation, and torsion) of the shaft. Whisker angles were defined by the orientation of the interpolated quadratic parametric curve in each frame. Details of these procedures follow below.

For calibration and estimation of camera position with respect to the rat, a standardized checkerboard image (8 × 8 patches of 4.5 × 4.5 mm) was used to generate a set of point correspondences. The MATLAB *Camera Calibration Toolbox* (http://www.vision.caltech.edu/bouguetj) was used to detect the corners of the checkerboard patches, with pixel coordinates $\boldsymbol{x}_i$ and $\boldsymbol{x}'_i$ in the two camera views. Twenty such images, with the checkerboard oriented differently in each image, were produced to yield a set of N point correspondences $(\boldsymbol{x}_i, \boldsymbol{x}'_i)$, $i = 1, \ldots, N$. Twenty images with 36 corners thus yielded $N = 720$ point correspondences. A fundamental result of epipolar geometry consists of the epipolar constraints, $\boldsymbol{x}'^T_i F \boldsymbol{x}_i = 0$, $i = 1, \ldots, N$, which relate point correspondences and where F is the fundamental matrix. The fundamental matrix encodes the epipolar geometry of the stereo camera pair and allows determination of the camera matrices, P and P', that encode the position, orientation, and intrinsic parameters of the cameras needed for the 3D reconstruction. An "*Eight Points*" algorithm (Hartley and Zisserman, 2000) (courtesy of Y. Wexler, Microsoft Research, Redmond) was applied to estimate F from the set of point correspondences. Three-dimensional reconstruction (up to a projective transformation) consisted of computing the 3D points $\boldsymbol{X}_i$ such that $\boldsymbol{x}_i = P\boldsymbol{X}_i$ and $\boldsymbol{x}'_i = P'\boldsymbol{X}_i$ for all $i = 1, \ldots, N$. The projective reconstruction was rectified to a metric reconstruction by the transformation matrix H. The latter was obtained from the 3D reconstruction of a scene (grid) that contained ground-control points (needles 5–30 mm in length) with known 3D positions. Estimated patch size of 3D reconstructed checkerboards was 4.52 ± 0.16 mm, demonstrating the high accuracy of our reconstruction method.

Bending and rigid motion (translation and rotation) of the whisker shaft were reconstructed relative to a head-centered coordinate system. In this coordinate system, the line connecting the right and left eyes was defined as the y axis, the x axis was defined orthogonal to the y axis (passing through the average position of the nostrils) and the z axis was chosen such that the system defined a right-handed coordinate system (Figure 1C). Whisker shapes were initially reconstructed in the coordinate system of the experimental setup and then transformed into the head-centered coordinate system, which was used for all further analysis. In the first frame f of each movie, a model whisker shape in the form of the quadratic parametric curve $\boldsymbol{X}(u) = \boldsymbol{a} + \boldsymbol{b}u + \boldsymbol{c}u^2$ was fitted to three reconstructed dye marks, where $\mathbf{X}(u) = (X(u), Y(u), Z(u))$, $u \in [0, 1]$ is the position vector of a whisker point in the head-centered coordinate system. The constant vectors $\boldsymbol{a}$, $\boldsymbol{b}$, $\boldsymbol{c}$ were determined in the first frame ($f = 1$) and then reused across all remaining frames of the same movie ($f = 2, \ldots, K$). If $\boldsymbol{U}$ and $\boldsymbol{W}$ denote the 3D coordinates of the most inward and outward dye marks, and $\boldsymbol{V}$ the 3D coordinates of the intermediate mark in one video frame, then the shape parameters $\boldsymbol{a}$, $\boldsymbol{b}$, and $\boldsymbol{c}$ in frame $f = 1$ were specified by the conditions $\boldsymbol{X}(0) = \boldsymbol{U}$, $\boldsymbol{X}(u_1) = \boldsymbol{V}$ and $\boldsymbol{X}(1) = \boldsymbol{W}$. The unknown parameter u_1 was determined by a smoothness condition of the form

$$\int_0^1 \left| \frac{d\boldsymbol{X}(u)}{du} \right|^2 du \rightarrow \min$$

that resulted in a cubic equation for $u_1 (0 < u_1 < 1)$. The 3D whisker model was extrapolated toward the whisker base and tip by increasing the definition interval of the curve parameter u. The whisker-shape model was validated by visually inspecting the 3D shapes reprojected back onto the raw video data.

The position vector of the whisker base in each frame f defined translational movement of the whisker. The orientation of the whisker was computed with respect to a reference whisker configuration, $\boldsymbol{X}_0(u)$, as follows. A plane was fitted to the whisker shape in frame $f = 1$ (the whisker defines a plane provided it is curved and has zero torsion; this torsion should not to be confused with the torsional angle of the whisker shaft. The torsion of a curve is an intrinsic shape

property and describes the amount of bending of the curve out of a plane). The whisker shape was then rotated such that the normal vector of the plane was aligned with the direction of the x axis and tangential to the y axis of the head-centered coordinate system. A general whisker configuration was then defined with respect to the reference whisker as the set of three successive rotations:

$$R(\theta,\varphi,\zeta) = R_z(\theta)R_x(\varphi)R_y(\zeta) \quad (1)$$

where

$$R_z(\theta) = \begin{pmatrix} \cos\theta & -\sin\theta & 0 \\ \sin\theta & \cos\theta & 0 \\ 0 & 0 & 1 \end{pmatrix}, R_x(\varphi) = \begin{pmatrix} 1 & 0 & 0 \\ 0 & \cos\varphi & \sin\varphi \\ 0 & -\sin\varphi & \cos\varphi \end{pmatrix},$$
$$R_y(\zeta) = \begin{pmatrix} \cos\zeta & 0 & -\sin\zeta \\ 0 & 1 & 0 \\ \sin\zeta & 0 & \cos\zeta \end{pmatrix} \quad (2)$$

and θ, φ, and ζ are the azimuthal, elevational, and torsional angles, respectively. Thus, when the whisker was in the reference configuration, all angles were zero, i.e., $\{\theta,\varphi,\zeta\} = 0$. The rotation angles of frame *f* were estimated by least-square minimization of the error function $[\boldsymbol{X}_f(u) - R(\theta,\varphi,\xi)\boldsymbol{X}_0(u)]^2$ using MATLAB.

SUPPLEMENTAL DATA

The Supplemental Data for this article can be found online at http://www.neuron.org/cgi/content/full/59/1/35/DC1/.

ACKNOWLEDGMENTS

We are most grateful to Maciej Pietr for his assistance with object localization experiments and helpful advice throughout experiments and analysis. Yonathan Wexler contributed code for computing the *F* matrix. Arnon Yohanan assisted during head-fixed experiments. Mitra Hartmann, Tony Prescott, Barbara Schick, Inbar Saraf-Sinik, and Avi Saig commented on drafts of the manuscript. This work was supported by the Israel Science Foundation grant #959/06, The Minerva Foundation funded by the Federal German Ministry for Education and Research, the United States-Israel Binational Science Foundation (BSF) grant 2003222, and the EU FP7 BIOTACT project (ICT-215910; www.biotact.org). E.A. holds the Helen Diller Family Professorial Chair of Neurobiology. The authors declare that no competing interests exist.

Received: August 27, 2007
Revised: March 13, 2008
Accepted: May 7, 2008
Published: July 9, 2008

REFERENCES

Andermann, M.L., Ritt, J., Neimark, M.A., and Moore, C.I. (2004). Neural correlates of vibrissa resonance; band-pass and somatotopic representation of high-frequency stimuli. Neuron *42*, 451–463.

Arabzadeh, E., Panzeri, S., and Diamond, M.E. (2004). Whisker vibration information carried by rat barrel cortex neurons. J. Neurosci. *24*, 6011–6020.

Arabzadeh, E., Zorzin, E., and Diamond, M.E. (2005). Neuronal encoding of texture in the whisker sensory pathway. PLoS Biol. *3*, e17.

Bermejo, R., Vyas, A., and Zeigler, H.P. (2002). Topography of rodent whisking–I. Two-dimensional monitoring of whisker movements. Somatosens. Mot. Res. *19*, 341–346.

Brecht, M., Preilowski, B., and Merzenich, M.M. (1997). Functional architecture of the mystacial vibrissae. Behav. Brain Res. *84*, 81–97.

Carvell, G.E., and Simons, D.J. (1990). Biometric analyses of vibrissal tactile discrimination in the rat. J. Neurosci. *10*, 2638–2648.

Carvell, G.E., and Simons, D.J. (1995). Task- and subject-related differences in sensorimotor behavior during active touch. Somatosens. Mot. Res. *12*, 1–9.

Dorfl, J. (1985). The innervation of the mystacial region of the white mouse: A topographical study. J. Anat. *142*, 173–184.

Ferezou, I., Haiss, F., Gentet, L.J., Aronoff, R., Weber, B., and Petersen, C.C. (2007). Spatiotemporal dynamics of cortical sensorimotor integration in behaving mice. Neuron *56*, 907–923.

Gao, P., Bermejo, R., and Zeigler, H.P. (2001). Whisker deafferentation and rodent whisking patterns: behavioral evidence for a central pattern generator. J. Neurosci. *21*, 5374–5380.

Gibson, J.M., and Welker, W.I. (1983). Quantitative studies of stimulus coding in first-order vibrissa afferents of rats. 1. Receptive field properties and threshold distributions. Somatosens. Res. *1*, 51–67.

Hartley, R., and Zisserman, A. (2000). Multiple View Geometry in Computer Vision (Cambridge, UK: Cambridge University Press).

Herfst, L.J., and Brecht, M. (2008). Whisker movements evoked by stimulation of single motor neurons in the facial nucleus of the rat. J. Neurophysiol., in press. Published online March 19, 2008. 10.1152/jn.01014.2007.

Jones, L.M., Depireux, D.A., Simons, D.J., and Keller, A. (2004). Robust temporal coding in the trigeminal system. Science *304*, 1986–1989.

Knutsen, P.M., Derdikman, D., and Ahissar, E. (2005). Tracking whisker and head movements in unrestrained behaving rodents. J. Neurophysiol. *93*, 2294–2301.

Knutsen, P.M., Pietr, M., and Ahissar, E. (2006). Haptic object localization in the vibrissal system: behavior and performance. J. Neurosci. *26*, 8451–8464.

Krupa, D.J., Matell, M.S., Brisben, A.J., Oliveira, L.M., and Nicolelis, M.A. (2001). Behavioral properties of the trigeminal somatosensory system in rats performing whisker-dependent tactile discriminations. J. Neurosci. *21*, 5752–5763.

Krupa, D.J., Wiest, M.C., Shuler, M.G., Laubach, M., and Nicolelis, M.A. (2004). Layer-specific somatosensory cortical activation during active tactile discrimination. Science *304*, 1989–1992.

Lichtenstein, S.H., Carvell, G.E., and Simons, D.J. (1990). Responses of rat trigeminal ganglion neurons to movements of vibrissae in different directions. Somatosens. Mot. Res. *7*, 47–65.

Ritt, J.T., Andermann, M.L., and Moore, C.I. (2008). Embodied information processing: vibrissa mechanics and texture features shape micromotions in actively sensing rats. Neuron *57*, 599–613.

Szwed, M., Bagdasarian, K., and Ahissar, E. (2003). Encoding of vibrissal active touch. Neuron *40*, 621–630.

Szwed, M., Bagdasarian, K., Blumenfeld, B., Barak, O., Derdikman, D., and Ahissar, E. (2006). Responses of trigeminal ganglion neurons to the radial distance of contact during active vibrissal touch. J. Neurophysiol. *95*, 791–802.

Timofeeva, E., Merette, C., Emond, C., Lavallee, P., and Deschenes, M. (2003). A map of angular tuning preference in thalamic barreloids. J. Neurosci. *23*, 10717–10723.

von Heimendahl, M., Itskov, P.M., Arabzadeh, E., and Diamond, M.E. (2007). Neuronal activity in rat barrel cortex underlying texture discrimination. PLoS Biol. *5*, e305.

Waite, P.M., and Jacquin, M.F. (1992). Dual innervation of the rat vibrissa: responses of trigeminal ganglion cells projecting through deep or superficial nerves. J. Comp. Neurol. *322*, 233–245.

Yu, C., Derdikman, D., Haidarliu, S., and Ahissar, E. (2006). Parallel thalamic pathways for whisking and touch signals in the rat. PLoS Biol. *4*, e124.